

000
001
002054
055
056

Multi-channel Weighted Nuclear Norm Minimization for Real Color Image Denoising

057
058
059003
004
005
006
007060
061
062
063

Anonymous ICCV submission

008
009
010
011064
065
066

Paper ID 572

012
013
014067
068
069

Abstract

015

070
071

The noise structures among the R, G, B channels of real images are quite different due to the preprocessing steps in digital camera pipelines. This makes the real image denoising problem much more complex than traditional grayscale image denoising. In this paper, we propose a multi-channel optimization model for real color image denoising. Specifically, we introduce a weighting matrix into the data term to process adaptively each part of R, G, B channels in the joint patches concatenated by corresponding patches in these channels. In the regularization term, we employ the weighted nuclear norm to exploit the non-local self similar property. The proposed multi-channel weighted nuclear norm minimization (MC-WNNM) model is much more complex than the standard WNNM model. To solve this new problem, we reformulate the MC-WNNM model into a linear equality-constrained problem and solve it under the alternating direction method of multipliers (ADMM) framework. Each alternative updating step has closed-form solution and the convergence results are given. Experiments on benchmark datasets demonstrate that the proposed model outperforms state-of-the-art denoising methods on synthetic as well as real-world noisy images.

038
039080
081

1. Introduction

040
041082
083

Image denoising is an important problem in enhancing the image quality in computer vision systems. The traditional grayscale image denoising problem aims to recover the clean image \mathbf{x} from the noisy observation $\mathbf{y} = \mathbf{x} + \mathbf{n}$, where \mathbf{n} is often assumed to be additive white Gaussian noise (AWGN). Most image denoising methods in this field either employ the non-local self similarity (NSS) of natural images [1–7] or learn generative or discriminative denoisers from paired natural clean images and synthetic noisy images [8–12]. Among these methods, the weighted nuclear norm minimization (WNNM) method achieves excellent denoising performance by exploiting the NSS property

via low rank regularization.

The real color image denoising problem is not a trivial extension from single channel (grayscale image) to multiple channels (color image). The reason is that the noise in standard RGB (sRGB) space, though could be modeled as AWGN, are with different variances for different channels [13] due to the on-board processing steps in digital camera pipelines [14, 15]. This makes the real color image denoising problem much more complex. Directly applying the denoising methods for grayscale images to each channel of color images separately would obtain bad performance [16]. There are several work [14, 16–20] proposed specifically for color image denoising. The method [17] first transforms the color images into the luminance/chrominance space such as YCbCr before denoising, but this would make the noise distribution more complex in color images. The methods of [16, 20] process the joint patches concatenated by the corresponding patches in R, G, B channels and treat equally the patches in different channels. This would generate false colors or artifacts [16]. The methods of [14, 18, 19] ignore the non-local self similarity property of natural images, and their performance would be largely depressed [2, 7].

In order to deal with the R, G, B channels in color images more effectively, different noise properties of different channels should be considered in solving real color image denoising problem. Besides, due to its expressive denoising performance, the WNNM model [7] is employed to exploit the NSS property of natural images. In this paper, we proposed a multi-channel WNNM model for real color image denoising. By introducing a weighting matrix to the WNNM model, the proposed multi-channel WNNM model no longer has closed-form solutions and more challenging to solve. By reformulating the proposed multi-channel WNNM model into a linear equality-constrained program with two variables, the relaxed problem can be solved under the alternating direction method of multipliers (ADMM) [21] framework. Each variable can be updated with closed-form solution [7, 22]. We also give the convergency results with detailed proof to guarantee a rational termination of the proposed algorithm.

108

2. Related Work

109

2.1. Weighted Nuclear Norm Minimization

110

As an extension to the nuclear norm minimization (NNM) model [23], the weighted nuclear norm minimization (WNNM) model [7] is described as

111

$$\min_{\mathbf{X}} \|\mathbf{Y} - \mathbf{X}\|_F^2 + \|\mathbf{X}\|_{\mathbf{w},*} \quad (1)$$

112

where $\|\mathbf{X}\|_{\mathbf{w},*} = \sum_i w_i \sigma_i(\mathbf{X})$ is the weighted nuclear norm of matrix \mathbf{X} , and $\mathbf{w} = [w_1, \dots, w_n]^\top, w_i \geq 0$ is the weight vector, $\sigma_i(\mathbf{X})$ is the i -th singular value of matrix \mathbf{X} . According to the Corollary 1 of [24], the problem (1) has closed-form solution if the weights are non-decreasing

113

$$\hat{\mathbf{X}} = \mathbf{U} \mathcal{S}_{\mathbf{w}/2}(\Sigma) \mathbf{V}^\top \quad (2)$$

114

where $\mathbf{Y} = \mathbf{U} \Sigma \mathbf{V}^\top$ is the singular value decomposition [25] of \mathbf{Y} and $\mathcal{S}_\tau(\bullet)$ is the generalized soft-thresholding operator with weight vector \mathbf{w} :

115

$$\mathcal{S}_{\mathbf{w}/2}(\Sigma_{ii}) = \max(\Sigma_{ii} - w_{ii}/2, 0) \quad (3)$$

116

Though having achieved excellent performance on grayscale image denoising, the WNNM model would generate false colors or artifacts [16], if being directly extended to real color image denoising by processing each channel separately or joint vectors concatenated by multiple channels. In this paper, for real noisy image denoising, we propose a multi-channel WNNM model which preserve the power of WNNM and be able to process the differences among different channels.

117

2.2. Real Color Image Denoising

118

During the last decade, several denoising methods are proposed for real color image denoising [17–20]. Among them, the CBM3D [17] first transform the RGB image into luminance-chrominance space (e.g., YCbCr) and then apply the famous BM3D method [2] on each channel separately with the patches being grouped only in the luminance channel. In [18], the authors proposed the “Noise Level Function” to estimate and remove the noise for each channel in natural images. However, the methods processing each channel separately would achieve inferior performance than processing jointly these channels [16]. The methods of [19, 20, 26] perform real color image denoising by concatenating the patches in R, G, B channels into joint vectors. However, the concatenation would treat each channel equally and ignore the different noise properties among these channels. The method in [14] models the cross-channel noise in real noisy image as a multivariate Gaussian and the noise is removed by the Bayesian nonlocal means filter [27]. The commercial software Neat Image [28] estimates the noise parameters from a flat region of the given noisy image and filters the noise correspondingly. But

these methods [14, 28] ignore the non-local self similarity property of natural images [2, 7].

In this paper, we introduce a weighting matrix which add different weights to different channels for color image denoising. The proposed multi-channel method can effectively solve the problem of different noise structures among different channels.

3. Color Image Denoising via Multi-channel Weighted Nuclear Norm Minimization

3.1. The Problem

The color image denoising problem is to recover the clean image $\{\mathbf{x}_c\}$ from its noisy version $\mathbf{y}_c = \mathbf{x}_c + \mathbf{n}_c$, where $c \in \{r, g, b\}$ is the index of R, G, B channels and \mathbf{n}_c is the noise in c -th channel. The noise structures in each channel are different due to the on-board processing of the digital camera pipelines [15]. Therefore, it is problematic to directly apply denoising methods to the joint vectors concatenated by corresponding patches of the R, G, B channels. To validate this point, in Fig. 1, we show the clean image ‘‘kodim23’’ taken from the Kodak PhotoCD dataset, its degraded version generated by adding synthetic additive white Gaussian noise (AWGN) to each channel of ‘‘kodim23’’, and the denoised image by applying WNNM [7] on the joint vectors concatenated from R, G, B channels of the degraded image. The standard derivations of AWGN added to the R, G, B channels are $\sigma_r = 40$, $\sigma_g = 20$, $\sigma_b = 30$, respectively. The input standard derivation of the noise for the concatenated WNNM method is set as the Root Mean Square (RMS) of those in each channel, i.e., $\sigma = \sqrt{(\sigma_r^2 + \sigma_g^2 + \sigma_b^2)/3} = 31.1$. From Fig. 1, one can see that the concatenated WNNM method treating each channel equally would remain some noise in the R and B channel, while oversmoothing the G channel of the degraded image. Hence, if the patches of different channels are treated adaptively in the concatenated vectors, the degraded color images would be recovered with better visual qualities.

In order to process each channel differently while still exploiting the joint structures of the color images, in this paper, we introduce a weighting matrix \mathbf{W} to the concatenated WNNM method. Assume the matrix \mathbf{Y} containing the noisy patches in R, G, B channels as $\mathbf{Y} = [\mathbf{Y}_r^\top \mathbf{Y}_g^\top \mathbf{Y}_b^\top]^\top$, the corresponding clean matrix $\mathbf{X} = [\mathbf{X}_r^\top \mathbf{X}_g^\top \mathbf{X}_b^\top]^\top$, and the weights \mathbf{w} for the singular values of \mathbf{X} , then the proposed multi-channel WNNM (MC-WNNM) model is

$$\min_{\mathbf{X}} \|\mathbf{W}(\mathbf{Y} - \mathbf{X})\|_F^2 + \|\mathbf{X}\|_{\mathbf{w},*}. \quad (4)$$

How to set the weighting matrix \mathbf{W} and how to solve the proposed model will be introduced in the next sections.

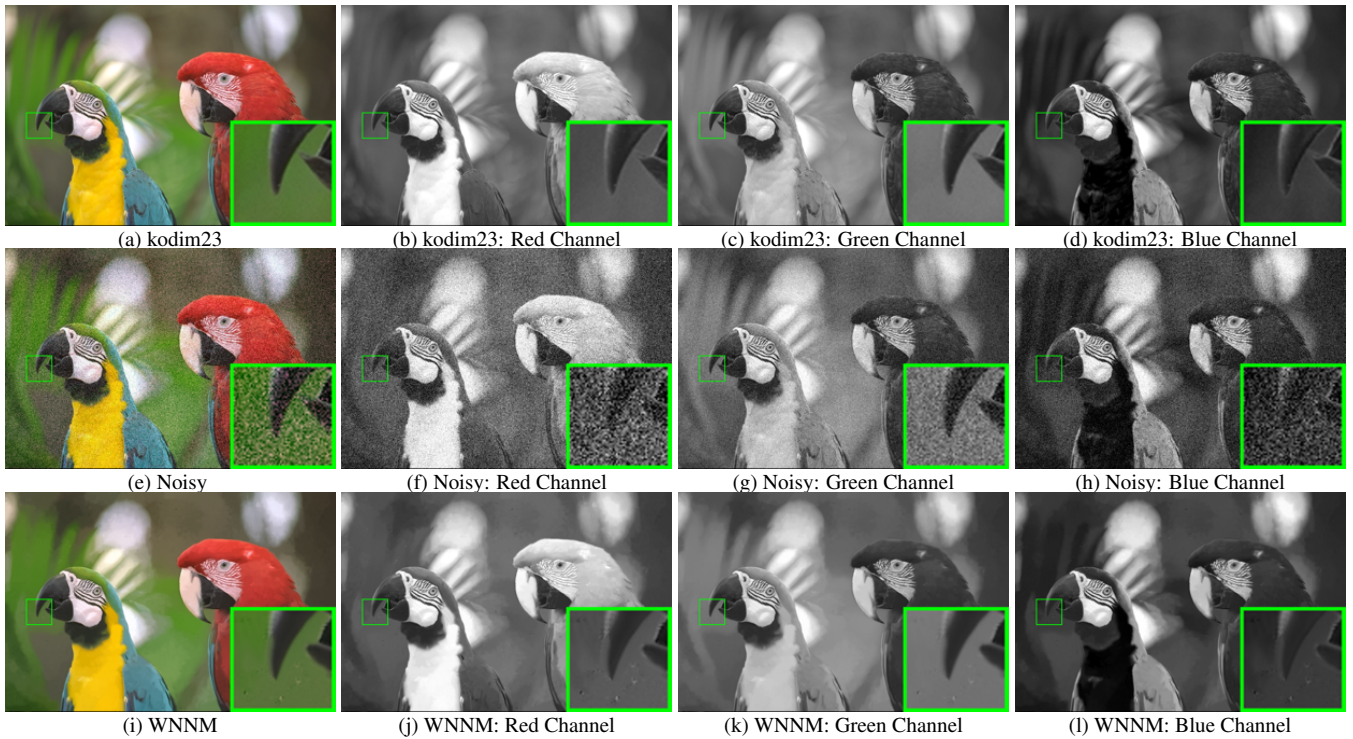


Figure 1. The image “kodim23” of the Kodak PhotoCD dataset, its degraded version, and the image recovered by WNNM. The R, G, B channels are also listed here for image quality comparison.

3.2. The Setting of Weighting Matrix \mathbf{W}

For simplicity, in this paper, we assume the noise are independent among the R, G, B channels and i.i.d. in each channel. Therefore, the weighting matrix \mathbf{W} is diagonal and can be determined under the Bayesian framework:

$$\begin{aligned} \hat{\mathbf{X}} &= \arg \max_{\mathbf{X}} \ln P(\mathbf{X}|\mathbf{Y}, \mathbf{w}) \\ &= \arg \max_{\mathbf{X}} \{\ln P(\mathbf{Y}|\mathbf{X}) + \ln P(\mathbf{X}|\mathbf{w})\}. \end{aligned} \quad (5)$$

The log-likelihood term $\ln P(\mathbf{Y}|\mathbf{X})$ is characterized by the statistics of noise, which is assumed to be channel-wise independent white Gaussian with standard deviations $\{\sigma_r, \sigma_g, \sigma_b\}$

$$P(\mathbf{Y}|\mathbf{X}) = \prod_{c \in \{r, g, b\}} (2\pi\sigma_c^2)^{-\frac{3p^2}{2}} \exp\left(-\frac{1}{2\sigma_c^2} \|\mathbf{Y}_c - \mathbf{X}_c\|_F^2\right). \quad (6)$$

We assume that the matrix \mathbf{X} follows the following distribution

$$P(\mathbf{X}|\mathbf{w}) \propto \exp\left(-\frac{1}{2} \|\mathbf{X}\|_{\mathbf{w},*}\right). \quad (7)$$

Putting (7) and (6) into (5), we have

$$\hat{\mathbf{X}} = \arg \min_{\mathbf{X}} \|\mathbf{W}(\mathbf{Y} - \mathbf{X})\|_F^2 + \|\mathbf{X}\|_{\mathbf{w},*}, \quad (8)$$

where

$$\mathbf{W} = \begin{pmatrix} \sigma_r^{-1} \mathbf{I} & \mathbf{0} & \mathbf{0} \\ \mathbf{0} & \sigma_g^{-1} \mathbf{I} & \mathbf{0} \\ \mathbf{0} & \mathbf{0} & \sigma_b^{-1} \mathbf{I} \end{pmatrix}. \quad (9)$$

where $\mathbf{I} \in \mathbb{R}^{p^2 \times p^2}$ is the identity matrix. Hence, the weighting matrix \mathbf{W} is determined to contribute equal weights for the pixel values in the same channel, while different weights for those in different channels. The experimental (which will be introduced later) results have already demonstrated that this form of weighting matrix have already generated the best denoising performance on synthetic and real noisy images in benchmark datasets.

3.3. The Denoising Algorithm

In this section, with the proposed MC-WNNM model, we propose a denoising algorithm for color images. In our algorithm, given a noisy image \mathbf{y} , each local patch is extracted from it with patch size $p \times p \times 3$ and stretched to a patch vector $\mathbf{y}_j \in \mathbb{R}^{3p^2}$ concatenated by corresponding patches in R, G, B, channels. Then we search the M most similar patches to \mathbf{y}_j (including \mathbf{y}_j itself) by Euclidean distance in a $W \times W$ local region around it. We stack the M similar patches column by column to form a noisy patch matrix $\mathbf{Y}_j = \mathbf{X}_j + \mathbf{N}_j \in \mathbb{R}^{3p^2 \times M}$, where \mathbf{X}_j and \mathbf{N}_j the corresponding clean and noise patch matrices. Then, we can apply the proposed MC-WNNM model to \mathbf{Y}_j to estimate \mathbf{X}_j for color image denoising:

$$\min_{\mathbf{X}_j} \|\mathbf{W}_j(\mathbf{Y}_j - \mathbf{X}_j)\|_F^2 + \|\mathbf{X}_j\|_{\mathbf{w},*}. \quad (10)$$

where \mathbf{W}_j is defined in Eq. (9). Just as [24] did, the weight vector \mathbf{w} is set $w_i^{k+1} = \frac{C}{|\sigma_i(\mathbf{X}_k)| + \epsilon}$ and $\epsilon > 0$ is a small

324 **Algorithm 1:** Color Image Denoising by MC-WNNM
 325 **Input:** Noisy image \mathbf{y} , noise levels $\{\sigma_r, \sigma_g, \sigma_b\}$;
 326 **Initialization:** $\hat{\mathbf{x}}^{(0)} = \mathbf{y}, \mathbf{y}^{(0)} = \mathbf{y}$;
 327 **for** $k = 1 : K_1$ **do**
 328 1. Set $\mathbf{y}^{(k)} = \hat{\mathbf{x}}^{(k-1)}$;
 329 2. Extracte local patches $\{\mathbf{y}_j\}_{j=1}^N$ from $\mathbf{y}^{(k)}$;
 330 **for** each patch \mathbf{y}_j **do**
 331 3. Search non-local similar patches \mathbf{Y}_j ;
 332 4. Apply the MC-WNNM model (10) to \mathbf{Y}_j and
 333 obtain the estimated \mathbf{X}_j ;
 334 **end for**
 335 5. Aggregate $\{\mathbf{X}_j\}_{j=1}^N$ to form the image $\hat{\mathbf{x}}^{(k)}$;
 336 **end for**
 337 **Output:** Denoised image $\hat{\mathbf{x}}^{K_1}$.

340 number to avoid zero numerator. Note that when $\sigma_r = \sigma_g =$
 341 σ_b , the multi-channel WNNM model will be reduced to the
 342 concatenated WNNM model as a special case.

343 The multi-channel WNNM is applied to the noisy patch
 344 matrix \mathbf{Y}_j of each local patch \mathbf{y}_j in the noisy image \mathbf{y} . And
 345 then all the patches are aggregated together to form the final
 346 recovered image $\hat{\mathbf{y}}$. To obtain better denoising results,
 347 we perform the above denoising procedure for several (K_1)
 348 iterations. The proposed MC-WNNM denoising algorithm
 349 for color images is summarized in Algorithm 1.

350 3.4. Optimization

351 The proposed MC-WNNM model could not be solved
 352 in an analytical form while the original WNNM model
 353 [24] could. In the WNNM model, when the weights on
 354 singular values are non-descending, the weighted nuclear
 355 norm proximal operator [24] can have global optimum with
 356 closed-form solution. However, such property is not valid
 357 for the multi-channel WNNM model. The reason is that the
 358 weighting matrix \mathbf{W} is added to the rows of matrix \mathbf{X} instead
 359 of its singular values. Besides, the elements in \mathbf{W} is
 360 not in a non-descending order with respect to the singular
 361 value of \mathbf{X} . This makes the proposed model more difficult
 362 to solve when compared to the original WNNM model.

363 By introducing an augmented variable \mathbf{Z} , the MC-
 364 WNNM model is reformulated as a linear equality-
 365 constrained problem with two variables \mathbf{X} and \mathbf{Z} :

$$366 \min_{\mathbf{X}, \mathbf{Z}} \|\mathbf{W}(\mathbf{Y} - \mathbf{X})\|_F^2 + \|\mathbf{Z}\|_{w,*} \quad \text{s.t. } \mathbf{X} = \mathbf{Z}. \quad (11)$$

370 Since the objective function is separable across the two variables,
 371 the problem (11) can be solved under alternating direction
 372 method of multipliers (ADMM) framework. We can
 373 derive its augmented Lagrangian function:
 374

$$375 \mathcal{L}(\mathbf{X}, \mathbf{Z}, \mathbf{A}, \rho) = \|\mathbf{W}(\mathbf{Y} - \mathbf{X})\|_F^2 + \|\mathbf{Z}\|_{w,*} \\ 376 \quad + \langle \mathbf{A}, \mathbf{X} - \mathbf{Z} \rangle + \frac{\rho}{2} \|\mathbf{X} - \mathbf{Z}\|_F^2 \quad (12)$$

378 where \mathbf{A} is the augmented Lagrangian multiplier and $\rho > 0$
 379 is the penalty parameter. We initialize the matrix variables
 380 \mathbf{X}_0 , \mathbf{Z}_0 , and \mathbf{A}_0 to be zero matrix of suitable size. By tak-
 381 ing derivative of the Lagrangian function \mathcal{L} with respect to
 382 the variables \mathbf{X} and \mathbf{Z} and setting the derivative function to
 383 be zero, we can alternatively update the ADMM algorithm
 384 iteratively as follows:

385 (1) **Update \mathbf{X} while fixing \mathbf{Z} and \mathbf{A} :**

$$386 \mathbf{X}_{k+1} = \arg \min_{\mathbf{X}} \|\mathbf{W}(\mathbf{Y} - \mathbf{X})\|_F^2 + \frac{\rho_k}{2} \|\mathbf{X} - \mathbf{Z}_k + \rho_k^{-1} \mathbf{A}_k\|_F^2 \quad (13)$$

387 This is a standard least squares regression problem with
 388 closed-form solution:

$$389 \mathbf{X}_{k+1} = (\mathbf{W}^\top \mathbf{W} + \frac{\rho_k}{2} \mathbf{I})^{-1} (\mathbf{W}^\top \mathbf{W} \mathbf{Y} + \frac{\rho_k}{2} \mathbf{Z}_k - \frac{1}{2} \mathbf{A}_k) \quad (14)$$

390 (2) **Update \mathbf{Z} while fixing \mathbf{X} and \mathbf{A} :**

$$391 \mathbf{Z}_{k+1} = \arg \min_{\mathbf{Z}} \frac{\rho_k}{2} \|\mathbf{Z} - (\mathbf{X}_{k+1} + \rho_k^{-1} \mathbf{A}_k)\|_F^2 + \|\mathbf{Z}\|_{w,*} \quad (15)$$

392 According to the Theorem 1 in [24], given the $\mathbf{X}_{k+1} +$
 393 $\rho_k^{-1} \mathbf{A}_k = \mathbf{U}_k \Sigma_k \mathbf{V}_k^\top$ be the SVD of $\mathbf{X}_{k+1} + \rho_k^{-1} \mathbf{A}_k$,
 394 where $\Sigma_k = \begin{pmatrix} \text{diag}(\sigma_1, \sigma_2, \dots, \sigma_n) \\ \mathbf{0} \end{pmatrix} \in \mathbb{R}^{m \times n}$, then the
 395 global optimum of the above problem is $\hat{\mathbf{Z}} = \mathbf{U}_k \hat{\Sigma}_k \mathbf{V}_k^\top$,
 396 where $\hat{\Sigma}_k = \begin{pmatrix} \text{diag}(\hat{\sigma}_1, \hat{\sigma}_2, \dots, \hat{\sigma}_n) \\ \mathbf{0} \end{pmatrix} \in \mathbb{R}^{m \times n}$ and
 397 $(\hat{\sigma}_1, \hat{\sigma}_2, \dots, \hat{\sigma}_n)$ is the solution to the following convex optimi-
 398 zation problem:

$$399 \min_{\hat{\sigma}_1, \hat{\sigma}_2, \dots, \hat{\sigma}_n} \sum_{i=1}^n (\sigma_i - \hat{\sigma}_i)^2 + \frac{2w_i}{\rho_k} \hat{\sigma}_i \quad (16)$$

400 s.t. $\hat{\sigma}_1 \geq \hat{\sigma}_2 \geq \dots \geq \hat{\sigma}_n \geq 0$.

401 According to the Remark 1 in [24], the problem above has
 402 closed-form solution

$$403 \hat{\sigma}_i = \begin{cases} 0 & \text{if } c_2 < 0 \\ \frac{c_1 + \sqrt{c_2}}{2} & \text{if } c_2 \geq 0 \end{cases} \quad (17)$$

404 where $c_1 = \sigma_i - \epsilon$, $c_2 = (\sigma_i - \epsilon)^2 - \frac{8C}{\rho_k}$ and C is set as
 405 $\sqrt{2n}$ by experience in image denoising.

406 (3) **Update \mathbf{A} while fixing \mathbf{X} and \mathbf{Z} :**

$$407 \mathbf{A}_{k+1} = \mathbf{A}_k + \rho_k (\mathbf{X}_{k+1} - \mathbf{Z}_{k+1}) \quad (18)$$

408 (4) **Update ρ_k :** $\rho_{k+1} = \mu * \rho_k$, where $\mu > 1$.

409 The above alternative updating steps are repeated until
 410 the convergence condition is satisfied or the number of
 411 iterations exceeds a preset maximum number, e.g., K_2 .
 412 The convergence condition of the ADMM algorithm is:
 413 $\|\mathbf{X}_{k+1} - \mathbf{Z}_{k+1}\|_F \leq \text{Tol}$, $\|\mathbf{X}_{k+1} - \mathbf{X}_k\|_F \leq \text{Tol}$, and
 414 $\|\mathbf{Z}_{k+1} - \mathbf{Z}_k\|_F \leq \text{Tol}$ are simultaneously satisfied, where

Algorithm 2: Solve MC-WNNM via ADMM

Input: Matrices \mathbf{Y} and \mathbf{W} , $\mu > 1$, $\text{Tol} > 0$;

Initialization: $\mathbf{X}_0 = \mathbf{Z}_0 = \mathbf{A}_0 = \mathbf{0}$, $\rho_0 > 0$, $\text{T} = \text{False}$, $k = 0$;

While ($\text{T} == \text{false}$) **do**

1. Update \mathbf{X}_{k+1} as

$$\mathbf{X}_{k+1} = (\mathbf{W}^\top \mathbf{W} + \frac{\rho_k}{2} \mathbf{I})^{-1} (\mathbf{W}^\top \mathbf{W} \mathbf{Y} + \frac{\rho_k}{2} \mathbf{Z}_k - \frac{1}{2} \mathbf{A}_k)$$
2. Update \mathbf{Z}_{k+1} by solving the problem

$$\min_{\mathbf{Z}} \frac{\rho_k}{2} \|\mathbf{Z}\|_F^2 + \|\mathbf{Z}\|_{w,*}$$
3. Update \mathbf{A}_{k+1} as $\mathbf{A}_{k+1} = \mathbf{A}_k + \rho_k (\mathbf{X}_{k+1} - \mathbf{Z}_{k+1})$
4. Update $\rho_{k+1} = \mu * \rho_k$;
5. $k \leftarrow k + 1$;
if (Convergence conditions are satisfied) or ($k \geq K_2$)
5. $\text{T} \leftarrow \text{True}$
end if

end while

Output: Matrices \mathbf{X} and \mathbf{Z} .

Tol > 0 is a small tolerance. We summarize the optimization steps in Algorithm 2. The convergence analysis of the proposed Algorithm 2 is given in Theorem 1. Note that since the weighted nuclear norm is non-convex in general, we employ an unbounded sequence of $\{\rho_k\}$ here to make sure that the Algorithm 2 is convergent.

Theorem 1. Assume the weights in w are in a non-descending order, the sequence $\{\mathbf{X}_k\}$, $\{\mathbf{Z}_k\}$, and $\{\mathbf{A}_k\}$ generated in Algorithm 1 satisfy:

$$(a) \lim_{k \rightarrow \infty} \|\mathbf{X}_{k+1} - \mathbf{Z}_{k+1}\|_F = 0; \quad (19)$$

$$(b) \lim_{k \rightarrow \infty} \|\mathbf{X}_{k+1} - \mathbf{X}_k\|_F = 0; \quad (20)$$

$$(c) \lim_{k \rightarrow \infty} \|\mathbf{Z}_{k+1} - \mathbf{Z}_k\|_F = 0. \quad (21)$$

Proof. We give proof sketch here and detailed proof of this theorem can be found in supplementary files. We can first proof that the sequence $\{\mathbf{A}_k\}$ generated by Algorithm 3.4 is upper bounded. Since $\{\rho_k\}$ is unbounded, that is $\lim_{k \rightarrow \infty} \rho_k = +\infty$, we can proof that the sequence of Lagrangian function $\{\mathcal{L}(\mathbf{X}_{k+1}, \mathbf{Z}_{k+1}, \mathbf{A}_k, \rho_k)\}$ is also upper bounded. Hence, both $\{\mathbf{W}(\mathbf{Y} - \mathbf{X}_k)\}$ and $\{\mathbf{Z}_k\}$ are upper bounded. According to Eq. (18), we can proof that $\lim_{k \rightarrow \infty} \|\mathbf{X}_{k+1} - \mathbf{Z}_{k+1}\|_F = \lim_{k \rightarrow \infty} \rho_k^{-1} \|\mathbf{A}_{k+1} - \mathbf{A}_k\|_F = 0$, and (a) is proofed. Then we can proof that $\lim_{k \rightarrow \infty} \|\mathbf{X}_{k+1} - \mathbf{X}_k\|_F \leq \lim_{k \rightarrow \infty} \|(\mathbf{W}^\top \mathbf{W} + \frac{\rho_k}{2} \mathbf{I})^{-1} (\mathbf{W}^\top \mathbf{W} \mathbf{Y} - \mathbf{W}^\top \mathbf{W} \mathbf{Z}_k - \frac{1}{2} \mathbf{A}_k)\|_F + \rho_k^{-1} \|\mathbf{A}_k - \mathbf{A}_{k-1}\|_F = 0$ and hence (b) is proofed. Then (c) can be proofed by checking that $\lim_{k \rightarrow \infty} \|\mathbf{Z}_{k+1} - \mathbf{Z}_k\|_F \leq \lim_{k \rightarrow \infty} \|\Sigma_{k-1} - S_{w/\rho_{k-1}}(\Sigma_{k-1})\|_F + \|\mathbf{X}_{k+1} - \mathbf{X}_k\|_F + \rho_k^{-1} \|\mathbf{A}_{k-1} + \mathbf{A}_{k+1} - \mathbf{A}_k\|_F = 0$, where $\mathbf{U}_{k-1} \Sigma_{k-1} \mathbf{V}_{k-1}^\top$ is the SVD of the matrix $\mathbf{X}_k + \rho_{k-1} \mathbf{A}_{k-1}$. \square

4. Experiments

We evaluate the proposed MC-WNNM method on synthetic and real color image denoising. We compare the proposed method with other state-of-the-art denoising methods including CBM3D [17], MLP [10], WNNM [7], TNRD [12], “Noise Clinic” (NC) [19, 26], and the commercial software Neat Image (NI) [28].

4.1. Implementation Details

In synthetic experiments, the noise levels in R, G, B channels are assumed to be known as $\sigma_r, \sigma_g, \sigma_b$. In the real cases, the noise levels in R, G, B channels can be estimated via noise estimation methods [29, 30]. In this paper, we employ the method of [30] for its state-of-the-art performance. For the CBM3D method [17], the input noise levels are the Root Mean Square (RMS) as

$$\sigma = \sqrt{(\sigma_r^2 + \sigma_g^2 + \sigma_b^2)/3}. \quad (22)$$

For the methods of MLP [10] and TNRD [12], we retrain the models on grayscale images following their corresponding strategies at different noise levels from $\sigma = 5$ to $\sigma = 75$ with gap of 5. The denoising on color images is performed by processing separately each channel with the model trained at the same (or nearest) noise levels. NC [19, 26] is a blind image denoising method, so we just submit the noisy images (synthetic or real) to [26] and perform denoising using the default parameters. NI [28] is a commercial software suitable for real image denoising, while the code of CC [14] is not released (but its results on the 15 real noisy images in [14] are available by requesting the authors). Hence, we only compare with CC and NI in real image denoising experiments, and do not compare with them in synthetic experiments.

In order to take fully comparison with the original WNNM method [24], we extended the WNNM method [24] for color image denoising in three directions: 1) we apply the WNNM method [24] on each channel separately with corresponding noise levels $\sigma_r, \sigma_g, \sigma_b$. We call this method “WNNM0”; 2) we perform denoising on the joint vectors concatenated by corresponding patches in the R, G, B channels, where the input noise level σ is computed by RMS (Eq. (22)). We call this method “WNNM1”; 3) we set the weighting matrix \mathbf{W} in the proposed MC-WNNM model as $\mathbf{W} = \sigma^{-1} \mathbf{I}$. For fair comparison, we tune all these methods set the same parameters for “WNNM2” and the proposed MC-WNNM methods while achieving the best performance of “WNNM2”. For fair comparison, we tune the methods of “WNNM0”, “WNNM1”, “WNNM2”, and the proposed MC-WNNM to achieve corresponding best denoising performance (i.e., highest average PSNR results).

540

4.2. Experiments on Synthetic Noisy Images

In this section, we compare the proposed MC-WNNM method with other competing method [10, 12, 17, 19, 28] as well as the three extensions of WNNM [24] on the 24 high quality color images from the Kodak PhotoCD Dataset (<http://r0k.us/graphics/kodak/>), which are shown in Fig. 2. The noisy images are generated by adding additive white Gaussian noise (AWGN) with known standard derivations $\sigma_r, \sigma_g, \sigma_b$ for the R, G, B channels, respectively. In this paper, the noise levels we add to each channel of the 24 color images are $\sigma_r = 40, \sigma_g = 20, \sigma_b = 30$, respectively. More experiments can be found in the supplementary files. For the methods of “WNNM2” and MC-WNNM, we set the patch size as $p = 6$, the number of non-local similar patches as $M = 70$, the window size for searching similar patches as $W = 20$, the updating parameter $\mu = 1.001$, the number of iterations in Algorithm 1 as $K_1 = 8$, the number of iterations in Algorithm 2 as $K_2 = 10$. For “WNNM2”, the initial penalty parameter is set as $\rho_0 = 10$, while for the proposed MC-WNNM model, the penalty parameter is set as $\rho_0 = 3$.

The PSNR results are listed in Table 1 of the compared methods including CBM3D [17], MLP [10], TNRD [12], NI [28], NC [19, 26], “WNNM0” [24], “WNNM1”, “WNNM2” and the proposed MC-WNNM methods. The best PSNR results are highlighted in bold. One can see that on all the 24 images, our method achieves the highest PSNR values over the competing methods. On average PSNR, our proposed method achieves 0.48dB improvements over the “WNNM0” method and outperforms the “WNNM2” by 1.09dB. Fig. 3 shows a scene denoised by the compared methods. We can see that CBM3D and NC would remain noise while MLP and TNRD would generate artifacts. The methods of “WNNM0”, “WNNM1”, “WNNM2” would over-smooth much the image. By using the proposed MC-WNNM model, our method preserves the structures (e.g., edges and textures) better across the R, G, B channels and generate less artifacts than other denoising methods, leading to visually pleasant outputs. More visual comparisons can be found in the supplementary files.

4.3. Experiments on Real Noisy Images

In this section, we compare the proposed MC-WNNM method with other competing methods on the 15 real noisy images (Fig. 4). We do not compare with the “WNNM0” method due to limited space and its inferior performance. The noisy images were collected under controlled indoor environment. Each scene was shot 500 times under the same camera and camera setting. The mean image of the 500 shots is roughly taken as the “ground truth”, with which the PSNR can be computed. Since the image size is very large (about 7000×5000) and the 11 scenes share repetitive con-



Figure 2. The 24 high quality color images from the Kodak PhotoCD Dataset.

tents, the authors of [14] cropped 15 smaller images (of size 512×512) to perform experiments. For each real noisy image, the noise levels in R, G, B channels are estimated by [30]. Since the noise levels are small in real noisy images, for the method of MLP [10] and TNRD [12], we apply the trained models of corresponding methods and choose the best denoising results (highest average PSNR values). Both methods achieves best results when setting the noise levels of the trained models from $\sigma = 10$.

We perform quantitative comparison on the 15 cropped images used in [14]. The PSNR results are listed in Table 2 of the compared methods including CBM3D [17], MLP [10], TNRD [12], NC [19, 26], NI [28], CC [14] (copied from [14]), “WNNM1”, “WNNM2”, and the proposed MC-WNNM method. The highest PSNR results are highlighted in bold. On average PSNR, the proposed MC-WNNM method achieves 0.44dB improvements over the “WNNM1” method and outperforms the state-of-the-art denoising method CC [14] by 0.83dB. On 10 out of the whole 15 images, the proposed MC-WNNM method achieves the highest PSNR values. Both CC and “WNNM1” achieves highest PSNR results on 2 of 15 images. It should be noted that in the CC method, a specific model is trained for each camera and camera setting, while our method uses the same model for all images. Fig. 5 shows the denoised images of a scene captured by Canon 5D Mark 3 at ISO = 3200. We can see that CBM3D, NC, NI and CC would either remain noise or generate artifacts, while TNRD over-smooth much the image. By using the proposed MC-WNNM model achieves better visual quality results than other methods. More visual comparisons can be found in the supplementary files.

5. Conclusion and Future Work

The real noisy images have different noise structures among the R, G, B channels due to the preprocessing steps of the digital camera pipelines in CCD or CMOS sensors. This makes the real image denoising problem much more complex than grayscale image denoising. In this paper, we proposed a noval multi-channel (MC) model for real color image denoising. By introducing a weighting ma-

Table 1. PSNR(dB) results of different denoising algorithms on 24 natural images.

| Image# | CBM3D | MLP | TNRD | NI | NC | WNNM0 | WNNM1 | WNNM2 | MC-WNNM |
|---------|-------|-------|-------|-------|-------|-------|-------|-------|--------------|
| 1 | 25.24 | 25.70 | 25.74 | 23.85 | 24.90 | 26.01 | 25.95 | 25.58 | 26.66 |
| 2 | 28.27 | 30.12 | 30.21 | 25.90 | 25.87 | 30.08 | 30.11 | 29.80 | 30.20 |
| 3 | 28.81 | 31.19 | 31.49 | 26.00 | 28.58 | 31.58 | 31.61 | 31.20 | 32.25 |
| 4 | 27.95 | 29.88 | 29.86 | 25.82 | 25.67 | 30.13 | 30.16 | 29.84 | 30.49 |
| 5 | 25.03 | 26.00 | 26.18 | 24.38 | 25.15 | 26.44 | 26.39 | 25.32 | 26.82 |
| 6 | 26.24 | 26.84 | 26.90 | 24.65 | 24.74 | 27.39 | 27.30 | 26.88 | 27.98 |
| 7 | 27.88 | 30.28 | 30.40 | 25.63 | 27.69 | 30.47 | 30.54 | 29.70 | 30.98 |
| 8 | 25.05 | 25.59 | 25.83 | 24.02 | 25.30 | 26.71 | 26.75 | 25.26 | 26.90 |
| 9 | 28.44 | 30.75 | 30.81 | 25.94 | 27.44 | 30.86 | 30.92 | 30.29 | 31.49 |
| 10 | 28.27 | 30.38 | 30.57 | 25.87 | 28.42 | 30.65 | 30.68 | 29.95 | 31.26 |
| 11 | 26.95 | 28.00 | 28.14 | 25.32 | 24.67 | 28.19 | 28.16 | 27.61 | 28.63 |
| 12 | 28.76 | 30.87 | 31.05 | 26.01 | 28.37 | 30.97 | 31.06 | 30.58 | 31.48 |
| 13 | 23.76 | 23.95 | 23.99 | 23.53 | 22.76 | 24.27 | 24.15 | 23.52 | 24.89 |
| 14 | 26.02 | 26.97 | 27.11 | 24.94 | 25.68 | 27.20 | 27.15 | 26.55 | 27.57 |
| 15 | 28.38 | 30.15 | 30.44 | 26.06 | 28.21 | 30.52 | 30.60 | 30.13 | 30.81 |
| 16 | 27.75 | 28.82 | 28.87 | 25.69 | 26.66 | 29.27 | 29.21 | 29.02 | 29.96 |
| 17 | 27.90 | 29.57 | 29.80 | 25.85 | 28.32 | 29.78 | 29.79 | 29.16 | 30.40 |
| 18 | 25.77 | 26.40 | 26.41 | 24.74 | 25.70 | 26.63 | 26.56 | 26.01 | 27.22 |
| 19 | 27.30 | 28.67 | 28.81 | 25.40 | 26.52 | 29.19 | 29.22 | 28.67 | 29.57 |
| 20 | 28.96 | 30.40 | 30.76 | 24.95 | 25.90 | 30.79 | 30.83 | 29.97 | 31.07 |
| 21 | 26.54 | 27.53 | 27.60 | 25.06 | 26.48 | 27.80 | 27.75 | 27.12 | 28.34 |
| 22 | 27.05 | 28.17 | 28.27 | 25.36 | 26.60 | 28.21 | 28.16 | 27.81 | 28.64 |
| 23 | 29.14 | 32.31 | 32.51 | 26.13 | 23.24 | 31.89 | 31.97 | 31.21 | 32.34 |
| 24 | 25.75 | 26.41 | 26.53 | 24.55 | 25.73 | 27.10 | 27.03 | 26.18 | 27.59 |
| Average | 27.13 | 28.54 | 28.68 | 25.24 | 26.19 | 28.84 | 28.83 | 28.22 | 29.31 |



Figure 3. Denoised images of different methods on the image “kodim07” degraded by noise with different levels on different channels. The images are better to be zoomed in on screen.

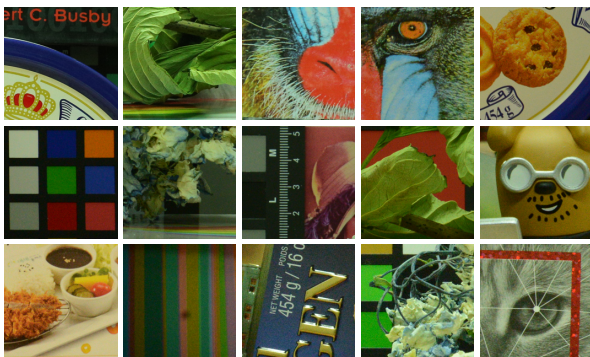


Figure 4. The 15 cropped real noisy images used in [14].

tri to the concatenated weighted nuclear norm minimization (WNNM) model, the proposed MC-WNNM model can process adaptively the different noise structures in each of the R, G, B channels and exploit the non-local self simi-

larity property of natural images. Though no longer having closed-form solution, we successfully solved the MC-WNNM model via an ADMM algorithm by reformulating the MC-WNNM model as a linear equality-constrained problem with two separable variables. We also studied the convergence property of the ADMM algorithm. Extensive experiments on synthetic and real color image denoising demonstrate that, the proposed MC-WNNM model outperforms the other competing denoising methods on both synthetic color noisy images as well as real-world noisy images. The introduce of the weighting matrix can boost the performance of traditional models on new applications. We believe that this work can be extended in at least two directions. Firstly, the weighting matrix beyond the diagonal form, such as correlation form [31], may bring better performance on color image denoising. Secondly, the proposed

Table 2. PSNR(dB) results of different methods on 15 cropped real noisy images used in [14].

| Camera Settings | CBM3D | MLP | TNRD | NI | NC | CC | WNNM1 | WNNM2 | MC-WNNM |
|---------------------------------|-------------------------|-------------------------|-------------------------|-------------------------|-------------------------|--------------------------------|-------------------------|-------------------------|--|
| Canon 5D Mark III ISO = 3200 | 39.76 36.40 36.37 | 39.00 36.34 36.33 | 39.51 36.47 36.45 | 35.68 34.03 32.63 | 36.20 34.35 33.10 | 38.37 35.37 34.91 | 39.74 35.12 33.14 | 39.98 36.65 34.63 | 41.13 37.28 36.52 |
| Nikon D600 ISO = 3200 | 34.18 35.07 37.13 | 34.70 36.20 39.33 | 34.79 36.37 39.49 | 31.78 35.16 39.98 | 32.28 35.34 40.51 | 34.98 35.95 41.15 | 35.08 36.42 40.78 | 35.08 36.84 39.24 | 35.53 37.02 39.56 |
| Nikon D800 ISO = 1600 | 36.81 37.76 37.51 | 37.95 40.23 37.94 | 38.11 40.52 38.17 | 34.84 38.42 35.79 | 35.09 38.65 35.85 | 37.99 40.36 38.30 | 38.28 41.24 38.04 | 38.61 40.81 38.96 | 39.26 41.43 39.55 |
| Nikon D800 ISO = 3200 | 35.05 34.07 34.42 | 37.55 35.91 38.15 | 37.69 35.90 38.21 | 38.36 35.53 40.05 | 38.56 35.76 40.59 | 39.01 36.75 39.06 | 39.93 37.32 41.52 | 37.97 37.30 38.68 | 38.91 37.41 39.39 |
| Nikon D800 ISO = 6400 | 31.13 31.22 30.97 | 32.69 32.33 32.29 | 32.81 32.33 32.29 | 34.08 32.13 31.52 | 34.25 32.38 31.76 | 34.61 33.21 33.22 | 35.20 33.61 33.62 | 34.57 33.43 34.02 | 34.80 33.95 33.94 |
| Average | 35.19 | 36.46 | 36.61 | 35.33 | 35.65 | 36.88 | 37.27 | 37.12 | 37.71 |

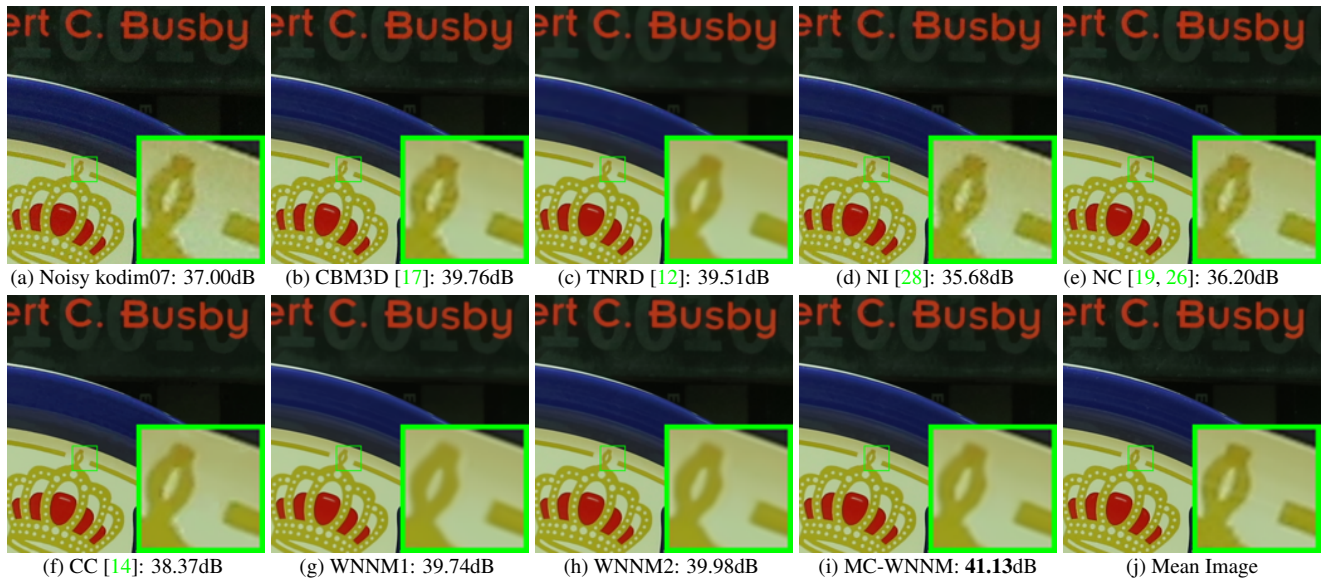


Figure 5. Denoised images of a region cropped from the real noisy image “Canon 5D Mark 3 ISO 3200 1” [14] by different methods. The images are better to be zoomed in on screen.

MC-WNNM model can be further extended to deal with hyperspectral images, which contain much more channels than color images.

References

- [1] A. Buades, B. Coll, and J. M. Morel. A non-local algorithm for image denoising. *IEEE Conference on Computer Vision and Pattern Recognition (CVPR)*, pages 60–65, 2005. 1
- [2] K. Dabov, A. Foi, V. Katkovnik, and K. Egiazarian. Image denoising by sparse 3-D transform-domain collabora-
- tive filtering. *IEEE Transactions on Image Processing*, 16(8):2080–2095, 2007. 1, 2
- [3] M. Elad and M. Aharon. Image denoising via sparse and redundant representations over learned dictionaries. *IEEE Transactions on Image Processing*, 15(12):3736–3745, 2006.
- [4] J. Mairal, F. Bach, J. Ponce, G. Sapiro, and A. Zisserman. Non-local sparse models for image restoration. *IEEE International Conference on Computer Vision (ICCV)*, pages 2272–2279, 2009.

- 864 [5] W. Dong, L. Zhang, G. Shi, and X. Li. Nonlocally central- 918
865 ized sparse representation for image restoration. *IEEE Trans- 919
866 actions on Image Processing*, 22(4):1620–1630, 2013. 920
867
- 868 [6] J. Xu, L. Zhang, W. Zuo, D. Zhang, and X. Feng. Patch 921
869 group based nonlocal self-similarity prior learning for image 922
870 denoising. *IEEE International Conference on Computer Vi- 923
871 sion (ICCV)*, pages 244–252, 2015. 924
872
- 873 [7] S. Gu, L. Zhang, W. Zuo, and X. Feng. Weighted nu- 925
874 clear norm minimization with application to image denois- 926
875 ing. *IEEE Conference on Computer Vision and Pattern 927
876 Recognition (CVPR)*, pages 2862–2869, 2014. 1, 2, 5
877 [8] S. Roth and M. J. Black. Fields of experts. *International 928
878 Journal of Computer Vision*, 82(2):205–229, 2009. 1
879
- 880 [9] D. Zoran and Y. Weiss. From learning models of natural 929
881 image patches to whole image restoration. *IEEE Interna- 930
882 tional Conference on Computer Vision (ICCV)*, pages 479– 931
883 486, 2011. 932
- 884 [10] H. C. Burger, C. J. Schuler, and S. Harmeling. Image 933
885 denoising: Can plain neural networks compete with BM3D? 934
886 *IEEE Conference on Computer Vision and Pattern Recog- 935
887 nition (CVPR)*, pages 2392–2399, 2012. 5, 6, 7
888
- 889 [11] U. Schmidt and S. Roth. Shrinkage fields for effective 936
890 image restoration. *IEEE Conference on Computer Vision and 937
891 Pattern Recognition (CVPR)*, pages 2774–2781, June 2014. 938
- 892 [12] Y. Chen, W. Yu, and T. Pock. On learning optimized 939
893 reaction diffusion processes for effective image restoration. 940
894 *IEEE Conference on Computer Vision and Pattern Recog- 941
895 nition (CVPR)*, pages 5261–5269, 2015. 1, 5, 6, 7, 8
896
- 897 [13] B. Leung, G. Jeon, and E. Dubois. Least-squares luma- 942
898 chroma demultiplexing algorithm for bayer demosaicking. 943
899 *IEEE Transactions on Image Processing*, 20(7):1885–1894, 944
900 2011. 1
901
- 902 [14] S. Nam, Y. Hwang, Y. Matsushita, and S. J. Kim. A holistic 945
903 approach to cross-channel image noise modeling and its ap- 946
904 plication to image denoising. *IEEE Conference on Computer 947
905 Vision and Pattern Recognition (CVPR)*, pages 1683–1691, 948
906 2016. 1, 2, 5, 6, 7, 8
907
- 908 [15] H. C. Karaimer and M. S. Brown. A software platform for 949
909 manipulating the camera imaging pipeline. *European Con- 950
910 ference on Computer Vision (ECCV)*, October 2016. 1, 2
911
- 912 [16] Julien Mairal, Michael Elad, and Guillermo Sapiro. Sparse 951
913 representation for color image restoration. *IEEE Transac- 952
914 tions on Image Processing*, 17(1):53–69, 2008. 1, 2
915
- 916 [17] K. Dabov, A. Foi, V. Katkovnik, and K. Egiazarian. Color 953
917 image denoising via sparse 3D collaborative filtering with 954
918 grouping constraint in luminance-chrominance space. *IEEE 955
919 International Conference on Image Processing (ICIP)*, pages 956
920 313–316, 2007. 1, 2, 5, 6, 7, 8
921
- [18] C. Liu, R. Szeliski, S. Bing Kang, C. L. Zitnick, and W. T. 922
923 Freeman. Automatic estimation and removal of noise from 924
924 a single image. *IEEE Transactions on Pattern Analysis and 925
925 Machine Intelligence*, 30(2):299–314, 2008. 1, 2
926
- [19] M. Lebrun, M. Colom, and J.-M. Morel. Multiscale image 927
927 blind denoising. *IEEE Transactions on Image Processing*, 928
928 24(10):3149–3161, 2015. 1, 2, 5, 6, 7, 8
929
- [20] F. Zhu, G. Chen, and P.-A. Heng. From noise modeling to 930
930 blind image denoising. *IEEE Conference on Computer Vi- 931
931 sion and Pattern Recognition (CVPR)*, June 2016. 1, 2
932
- [21] S. Boyd, N. Parikh, E. Chu, B. Peleato, and J. Eckstein. Dis- 933
933 tributed optimization and statistical learning via the alternat- 934
934 ing direction method of multipliers. *Found. Trends Mach. 935
935 Learn.*, 3(1):1–122, January 2011. 1
936
- [22] C. Lu, C. Zhu, C. Xu, S. Yan, and Z. Lin. Generalized sin- 937
937 gular value thresholding. *AAAI*, 2015. 1
938
- [23] J. Cai, E. J. Candès, and Z. Shen. A singular value thresh- 939
939 olding algorithm for matrix completion. *SIAM Journal on 940
940 Optimization*, 20(4):1956–1982, 2010. 2
941
- [24] S. Gu, Q. Xie, D. Meng, W. Zuo, X. Feng, and L. Zhang. 942
942 Weighted nuclear norm minimization and its applications to 943
943 low level vision. *International Journal of Computer Vision*, 944
944 pages 1–26, 2016. 2, 3, 4, 5, 6
945
- [25] C. Eckart and G. Young. The approximation of one matrix by 946
946 another of lower rank. *Psychometrika*, 1(3):211–218, 1936. 947
947 2
948
- [26] M. Lebrun, M. Colom, and J. M. Morel. The noise clinic: 949
949 a blind image denoising algorithm. [http://www.ipol.
950 im/pub/art/2015/125/](http://www.ipol.im/pub/art/2015/125/). Accessed 01 28, 2015. 2, 5,
951 6, 7, 8
952
- [27] C. Kervrann, J. Boulanger, and P. Coupé. Bayesian non- 953
953 local means filter, image redundancy and adaptive dictionar- 954
954 ries for noise removal. *International Conference on Scale 955
955 Space and Variational Methods in Computer Vision*, pages 956
956 520–532, 2007. 2
957
- [28] Neatlab ABSoft. Neat Image. [https://ni.
957 neatvideo.com/home](https://ni.neatvideo.com/home). 2, 5, 6, 8
958
- [29] X. Liu, M. Tanaka, and M. Okutomi. Single-image noise 959
959 level estimation for blind denoising. *IEEE Transactions on 960
960 Image Processing*, 22(12):5226–5237, 2013. 5
961
- [30] G. Chen, F. Zhu, and A. H. Pheng. An efficient statistical 962
962 method for image noise level estimation. *IEEE Interna- 963
963 tional Conference on Computer Vision (ICCV)*, December 2015. 5,
964 6
965
- [31] N. J. Higham. Computing the nearest correlation matrixa 966
966 problem from finance. *IMA Journal of Numerical Analysis*, 967
967 22(3):329, 2002. 7
968
- 969
- 970
- 971